

Article

Prediction of Ground Surface Settlements Induced by EPB Shield Tunneling in Water-Rich Soft Strata

Yi Yang ^{1,2} , Xinggao Li ^{1,2,*} , Dalong Jin ^{1,2}, Xingqi Jiang ³ and Hanyuan Li ^{1,2}

¹ Key Laboratory of Urban Underground Engineering of the Education Ministry, Beijing Jiaotong University, Beijing 100044, China; 17121139@bjtu.edu.cn (Y.Y.); jindalong@163.com (D.J.); 20115020@bjtu.edu.cn (H.L.)

² School of Civil Engineering, Beijing Jiaotong University, Beijing 100044, China

³ Changzhou Metro Group Co., Ltd., Changzhou 213000, China; xingqi_j@163.com

* Correspondence: lxg_njtu@163.com

Abstract: The main goal of this study is to enhance the prediction of ground surface settlements induced by Earth pressure balance (EPB) shield tunneling. In the setting of Changzhou, China, a comprehensive database of long-term ground-displacement findings from Metro Lines No. 1 and No. 2 was analyzed with the goal of assessing the parameters characterizing the settlement, i.e., volume loss, trough width parameter. For the metro lines in the water-rich soft strata of Changzhou, the ground loss V_l is usually in the range of 0.1–0.75%, and the trough width parameter K is usually in the range from 0.3 to 0.7. A superposition analytical method is proposed to estimate the short-term ground settlements induced by shield tunneling, with attention given to ground loss as well as shield working loads. The suggested analytical approach was found to be in good agreement with the field measurements in the case of EPB shield tunneling. This study can provide a reliable assessment of the long-term as well as short-term ground surface settlements for tunnel design.

Keywords: shield tunnel; metro; ground surface settlement; prediction model; settlement trough



Citation: Yang, Y.; Li, X.; Jin, D.; Jiang, X.; Li, H. Prediction of Ground Surface Settlements Induced by EPB Shield Tunneling in Water-Rich Soft Strata. *Appl. Sci.* **2022**, *12*, 4665. <https://doi.org/10.3390/app12094665>

Academic Editor: Daniel Dias

Received: 12 April 2022

Accepted: 3 May 2022

Published: 6 May 2022

Publisher's Note: MDPI stays neutral with regard to jurisdictional claims in published maps and institutional affiliations.



Copyright: © 2022 by the authors. Licensee MDPI, Basel, Switzerland. This article is an open access article distributed under the terms and conditions of the Creative Commons Attribution (CC BY) license (<https://creativecommons.org/licenses/by/4.0/>).

1. Introduction

The rapid construction of new infrastructure (including roads, railways, subways, etc.) has been, and will continue to be, a key process of urbanization in many countries. However, as the city grows, the available area for its expansion becomes restricted. In this context, the growth of underground space for infrastructure needs has achieved major developments in the last few decades. Despite significant technical and scientific developments, a crucial issue connected to tunneling in metropolitan regions persists. Ground movement induced by tunneling is unavoidable, which manifests as settling troughs at the ground surface, and many accidents, such as structural damage and ground collapse, may occur as a result of deformation.

The Earth pressure balance (EPB) shield method has been widely used in the development of urban underground space, especially in the subway systems [1]. Over the last few decades, the EPB shield method has shown high adaptability to different types of formations because of the advancements in soil conditioning technology [2,3]. However, predicting the magnitude and distribution of ground deformations induced by EPB shield driving, as well as assessing their effect on closely spaced structures, is a component of tunnel construction as significant as structural safety [4]. Various approaches, including on-site monitoring, analytical solutions, model tests, and numerical models, have been used to evaluate the ground displacement generated by shield driving. In terms of on-site monitoring, the surface deformation caused by the tunneling in the soft soil can be described in the form of a Gaussian curve, with the maximum settlement located above the tunnel centerline [5]. On the time scale of occurrence, this settlement trough can be distinguished into three types: short-term, medium-term, and long-term deformation [6], despite the fact that it might be difficult to tell them apart at times [7]. Based on the monitoring data, a series of empirical equations on the transversal

settlement profile were derived and became the most common assessment used in construction applications [8]. In addition to field monitoring, analytical methods mainly involve the elastic continuum approach and have been extensively used in the case of shield tunneling owing to their stringent framework [9]. Even for closed-form analytical solutions, some empirical parameters, such as ground loss, are required for accurate predictions, so they can also be called semiempirical methods. In addition, the model tests, as well as the numerical models, are often used to investigate the effect of a specific factor on settlement or for detailed analysis of a particularly complex case [10–12]. These methods may be time-consuming in assessing all conditions along a tunnel and lack the flexibility to provide quick feedback, leaving them impractical for engineers to use in less complex situations [13]. In recent years, artificial intelligence (AI) methods, such as artificial neural networks (ANNs), and some evolutionary algorithms, have been developed for tunneling-induced settlement prediction [14]. However, the accuracy of AI algorithms is strongly reliant on the considered datasets.

Hence, the empirical or semiempirical method remains the most common method for predicting tunneling-induced deformations, with the main advantage of higher prediction reliability based on a small number of input parameters. In this study, a classical empirical method for predicting the long-term deformation was used in a typical water-rich soft stratum. Based on the monitoring data collected from 59 cross sections, the prediction parameters in the empirical method and their variability were analyzed and summarized. Additionally, an analytical method was established and used to predict the short-term ground deformation induced by shield driving. A good agreement was observed between the proposed analytical method and the field measurements. This study provides a reference for assessing the long-term and short-term deformation induced by shield driving in the water-rich soft stratum.

2. Project Overview

2.1. Description of the Tunnel Project

Practical tunnel engineering in Changzhou, China, was considered to investigate the ground surface settlements induced by EPB shield tunneling. Changzhou city lies northwest of Shanghai and has a total area of 4373 km². Figure 1 describes the location and distribution of the rail track system in Changzhou. Nowadays, Changzhou Metro Lines No. 1 and No. 2 have opened with a total mileage of about 54 km in operation. EPB shield machines were employed to construct the tunnel section of the two opened metro lines. The shield tunnel length of Changzhou Metro is about 26 km in Line No. 1 and about 15 km in Line No. 2. Most shield tunnels were built with a buried depth in the range of 10 to 20 m, and the maximum depth reached was 27.5 m. Shield driving has an inevitable influence on the soft soils in Changzhou, resulting in ground loss and movement. A reliable prediction of tunneling-induced ground movements is of great importance for construction safety management.

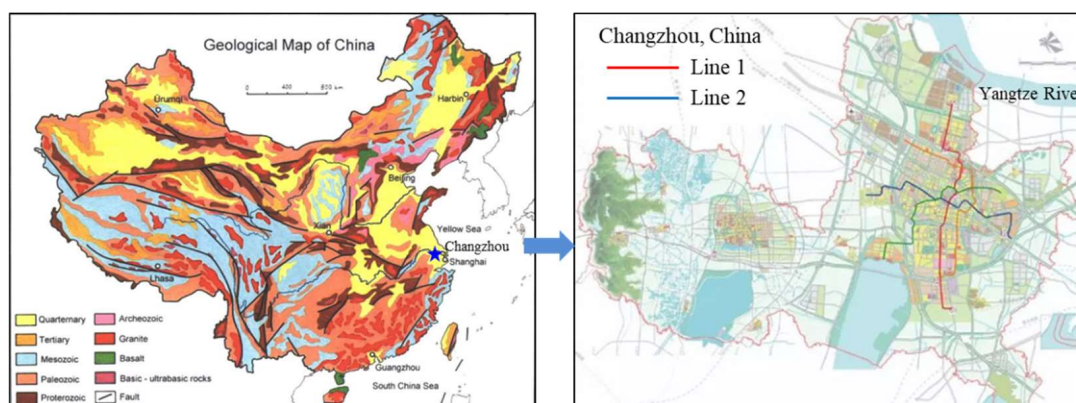


Figure 1. Location and distribution of the rail track system in Changzhou.

2.2. Geological and Geotechnical Conditions

The water-rich soft deposits of Changzhou were formed during the Pleistocene and Holocene epochs under the scouring of the Yangtze River and Taihu Lake. Figure 2 depicts the geological formation, soil types, and hydrogeology of the top 80.5 m deposit, which is the highest depth reached by human building operations. The deposit is a multiaquifer–aquitard system, as shown in Figure 2, with silty soil, clayey soil, and sandy soil overlapping. The deposit up to a depth of 80.5 m contains 10 geotechnical soil layers according to the soil properties and grain size distribution (labeled in circled numbers from ① to ⑩ in Figure 2). Each layer is further subdivided into sublayers on the basis of the color of the soil, for a total of 31 sublayers. The buried depth of each layer varies depending on its location.

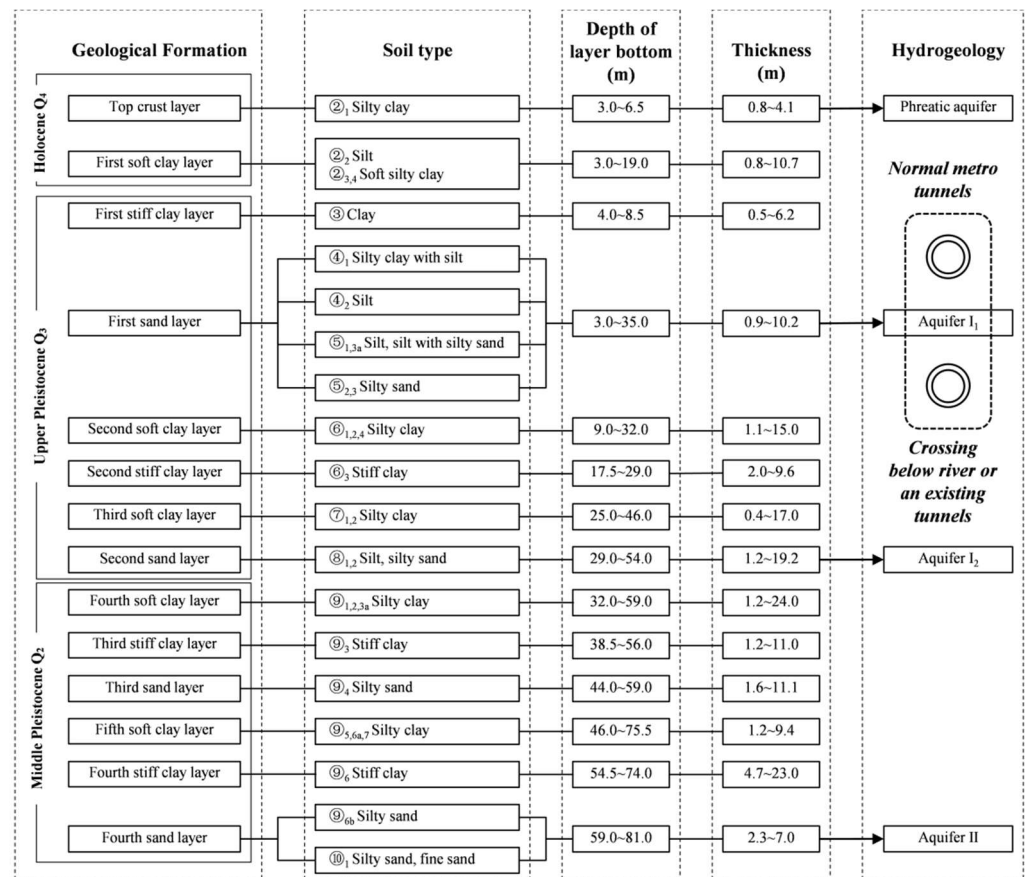


Figure 2. Geology and hydrogeology in Changzhou.

The geological and hydrogeological formation of each layer within the surveyed depth is described in the following. The top deposit is a top crust layer composed of silty clay, which is a phreatic aquifer with a groundwater level of 0.5–2.8 m below the surface. Following is a soft clay layer (the first soft clay layer). The top crust layer and the first soft clay layer were formed in the Holocene period. Next is a stiff clay layer (the first stiff clay layer). Underlying the first stiff clay layer is the first sand layer, which is mainly composed of silt and silty sand. Most normal metro tunnels are built in the first sand layer, and it is a low-pressure artesian aquifer (I₁) with a groundwater level of 3.15 to 5.45 m. The following layer is the second soft clay layer, which is a saturated and plastic layer with a high clay concentration. The second soft clay layer is the softest layer in Changzhou, where many below river crossing tunnels are built and are very sensitive to disturbance. The next layer is the second stiff clay layer, in which some below the river crossing tunnels are also built. The following are the third soft clay layer and the second sand layer, which are the deepest excavation positions for the EPB shield machine. The second sand layer contains a silt sublayer (⑧₁) and a silty sand sublayer (⑧₂). They are the second low-pressure artesian

aquifer (I_2), with a groundwater level from 4.23 to 8.13 m. Top to bottom, layers from the first stiff clay to the third soft clay layer were formed in the upper Pleistocene period, and they are the densely distributed areas of the metro lines. Deeper areas include several similar layers, such as soft clay layers, sand layers, and stiff clay layers, which were formed in the middle Pleistocene period, and they are usually located deeper than metro tunnels.

Figure 3 shows the geotechnical parameters of the water-rich soft strata in Changzhou. The physical parameters, including water content, unit weight, void ratio, plasticity index, and liquidity index, were determined using laboratory tests conducted in accordance with the Chinese standard [15], which is identical to the British Standard [16]. The compression index was determined using a normal oedometer test. Layers ⑤ and ⑧ are classed as sandy layers by the Unified Soil Classification because of their high sand content. The other layers with a significant silt concentration are classed as the clay layer. The permeability of clayey soils was determined using oedometer testing, and the permeability of the sandy soil was determined using pumping testing.

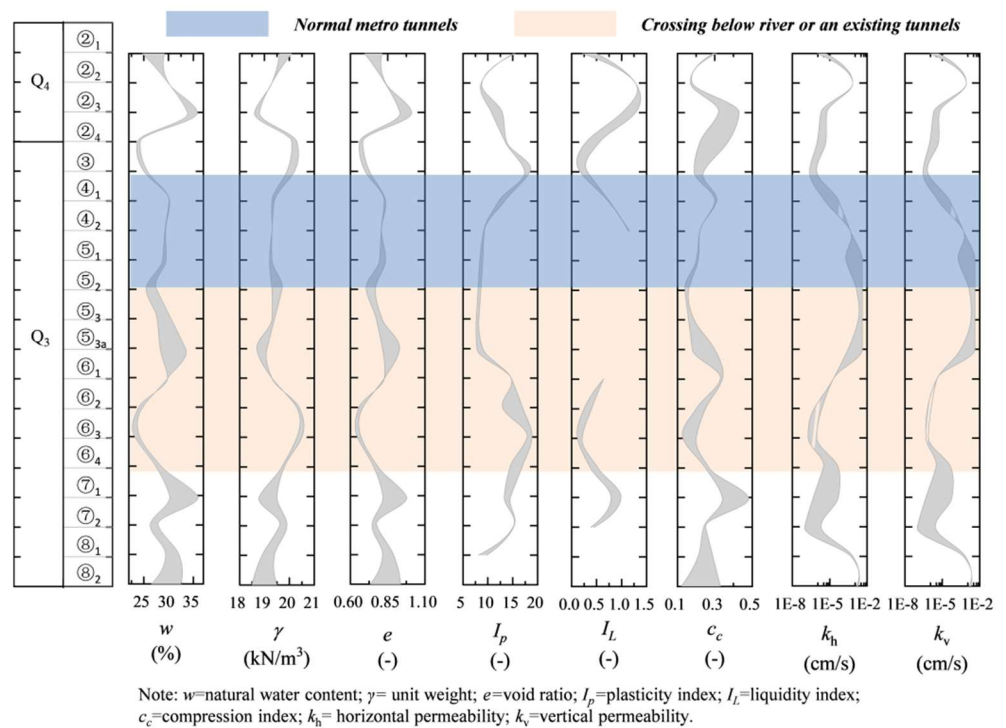


Figure 3. Soil profiles and geotechnical parameters of water-rich soft strata in Changzhou.

3. Prediction of Long-Term Settlement

3.1. Empirical Method

The empirical method first proposed by Peck (1969) [5] is the most widely used approach in predicting tunneling-induced surface settlements. As proposed by Peck (1969), an invert Gaussian distribution curve was advocated to describe the surface settlement trough caused by a single tunnel:

$$S(x) = S_{\max} \exp\left(-\frac{x^2}{2i^2}\right) \tag{1}$$

where $S(x)$ denotes the surface settlement at a distance x from the tunnel centerline, S_{\max} denotes the maximum surface settlement above the tunnel centerline, and i is called the trough width, which denotes the horizontal distance from the inflection point of the

settlement trough curve to the tunnel centerline. Because of the undrained condition in a typical EPB shield tunneling, the S_{max} can be written as:

$$S_{max} = \frac{0.313V_l D^2}{i} \tag{2}$$

where V_l denotes the volume loss defined as the amount of lost material caused by shield construction, and D denotes the diameter of the tunnel.

As described in Equation (2), two key parameters—volume loss V_l and trough width i —are required when applying the empirical method in engineering practice. According to Bloodworth (2002) [6], it is difficult to predict the volume loss V_l before tunnel construction since it is dependent on a number of unknown factors. The nature of the geological and geotechnical conditions is the most decisive factor that governs the V_l . As reported by O’Reilly and New (1982) [17], the trough width i is mostly connected to the buried depth, as well as the geological conditions, and is generally independent of the tunnel diameter or work quality. For the purpose of practical prediction, a linear relationship between the trough width i and the buried depth H was suggested by O’Reilly and New (1982):

$$i = KH \tag{3}$$

where K is called the trough width parameter. Since the volume loss V_l and the trough width parameter K are both closely related to local geological conditions, establishing a statistical relationship between them is of great importance in the surface settlement empirical prediction.

3.2. Statistics of Volume Loss

In the case of metro construction in Changzhou, the surface settlement data were carefully recorded and collected. The measured settlement data of 59 cross sections collected from Line 1 and Line 2 were used as a dataset. The S_{max} and i are obtained by performing Gaussian distribution fitting on the selected data. Then the V_l and K are converted using Equations (2) and (3). Figure 4a shows the distribution of volume loss V_l for different soil types. Because of the minor differences in shield diameter for different projects, the buried depth H was normalized by the tunnel diameter D , which is a common presentation way in other studies [18]. As given in Figure 4a, all of the observed V_l results are below 1.5%. It is clear that the V_l within $3H/D$ is lower than 1%. Beyond $3H/D$, the V_l of several cross sections exceeds 1%. It can be concluded that the highest V_l is more likely induced in the deeper silty sand layers, such as ⑤₂ and ⑤₃.

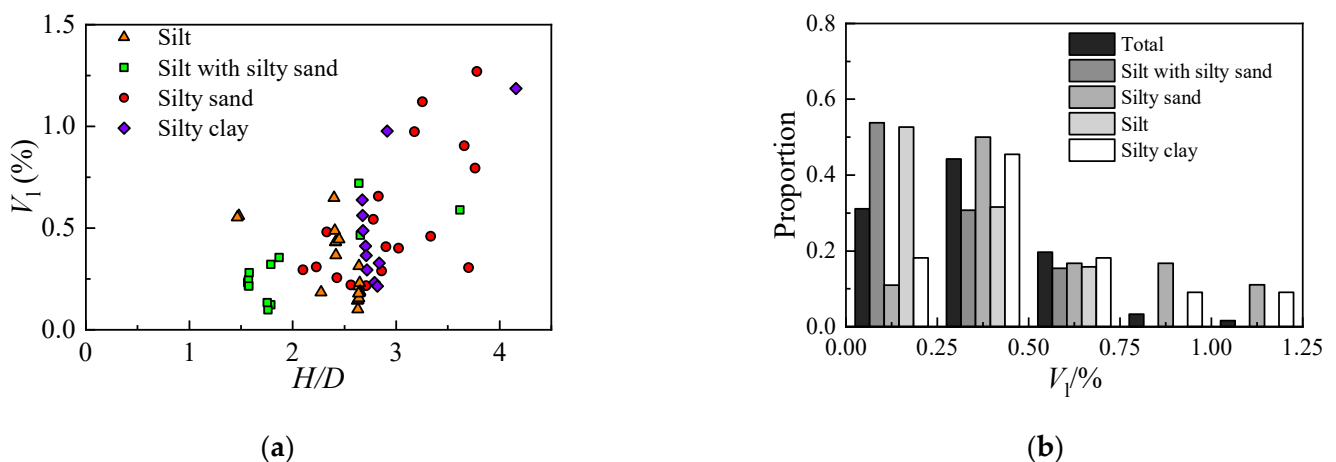


Figure 4. Statistical result of the volume loss V_l . (a) volume loss V_l vs. buried depth H , (b) probability distribution of V_l .

Figure 4b shows the statistics of the distribution of V_I for different ground types. What can be noticed is the fact that the silt with silty sand layer and silt layer shows no strong, obvious distinction. In general, most V_I induced in these layers is below 0.75%, with half of the results between 0 and 0.25% and 30% of the results between 0.25% and 0.50%. Not surprisingly, the V_I induced in silty sand is slightly higher than that in the silt layer, with more than 40% of the V_I exceeding 0.50%.

Although Figure 4 presents detailed statistics of V_I , it is still a challenge to predict V_I before construction as a lot of factors, such as the shield machine performance and the quality of work, are uncertain. Despite these difficulties, the empirical data in Figure 4 provide the basis for finding out the variability of V_I , which can aid in selecting its representative values for design objectives.

3.3. Statistics of Trough Width Parameter

Based on the data points of 59 cross sections, the relationship between trough width i and buried depth H for different soil types, in comparison with different reference lines of trough width parameter K , is shown in Figure 5a. For a common presentation, the buried depth H and trough width i were normalized by the tunnel diameter D . Based on linear regressions, the average value of trough width parameter K for each soil layer was estimated as follows: silt: $K = 0.40$, slit with silty sand: $K = 0.52$, silty sand: $K = 0.51$, and silty clay: $K = 0.42$. As can be observed, most data points are located in the range of 0.30–0.70.

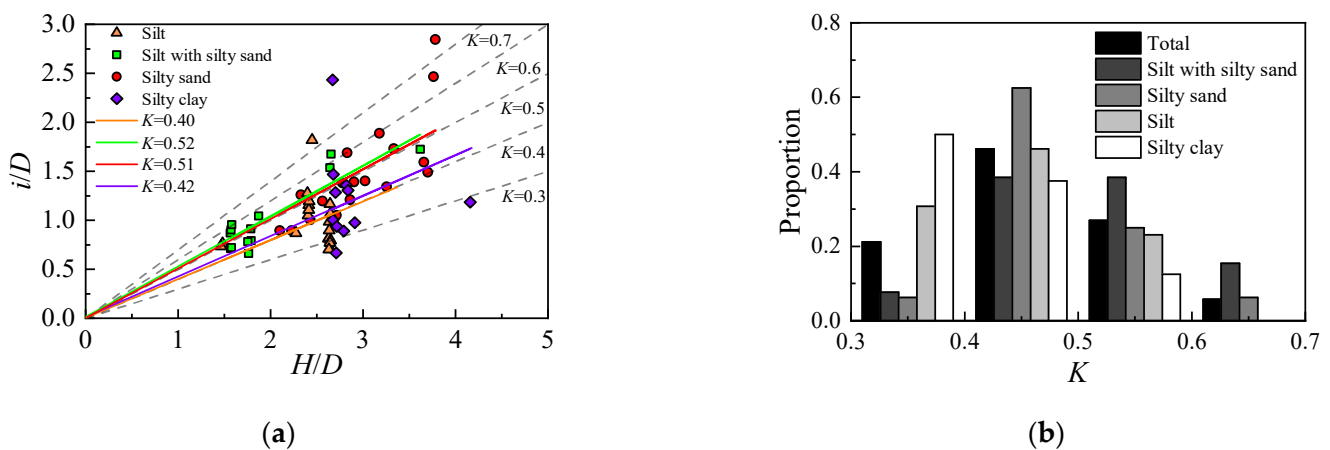


Figure 5. Statistical result of the trough width parameters K . (a) trough width parameter K vs. buried depth H , (b) probability distribution of K .

For a better overview of the parameter K , Figure 5b presents the histograms distribution of the trough width parameter K . In comparison, cohesion soils (silty clay or silt) show a little lower K than cohesionless soils (silty sand or silt with silty sand), but also with a higher scatter of results. This may be attributed to the intrinsic unpredictability of the parameter K for the cohesion soil in Changzhou, as well as the limits of the database used in this study. For cohesionless soils (silt with silty sand and silty sand), the K value ranges mostly between 0.40–0.60. In the case of cohesion soils (Silty clay or Silt), the K value is primarily in the range of 0.30–0.60.

The observed statistics on V_I and K can serve as a foundation for more reasonable, statistically driven predictions for long-term ground settlement for future EPB shield tunneling in similar water-rich soft strata.

4. Prediction of Short-Term Ground Deformation

Using the empirical method described in Section 2, a reliable prediction for the long-term settlement can be carried out. However, the ground deformation that occurred during the shield tunneling (i.e., short-term) is also the main concern in practice, especially in

the urban water-rich soft strata such as Changzhou. Many accidents, such as structural damage or ground collapse, could occur because of a lack of well-controlled TBM drive. In this section, an accurate prediction method for three-dimensional ground deformation during shield driving is established.

4.1. Interaction between EPB Shield Machine and Soil

As suggested by Leca & New (2007) [19], the effect of shield driving on the surrounding soils can be divided into two separate parts, ground loss and working loads. Figure 6 gives a brief description of the interaction between the EPB shield machine and soil. The ground loss induced by shield tunneling is caused primarily by the following factors: overexcavation caused by shield conicity, the tail void between shield and lining, and the deformations of the lining. The working loads consist of three parts, namely face support pressure, shield shell friction, and cutter head rotation, as described in Figure 6. In this study, a three-dimensional superposition method is suggested to obtain the short-term ground deformation induced by shield tunneling. In the proposed method, the cavity expansion theory and Mindlin's solution are used to calculate the displacements caused by ground loss and working loads, respectively.

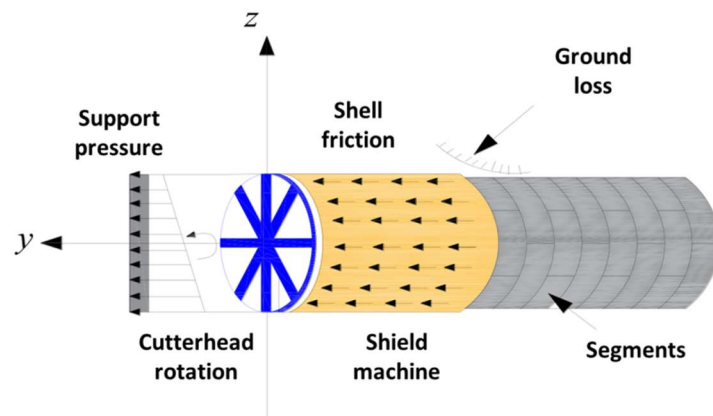


Figure 6. Interaction between the EPB shield machine and soil.

4.2. Deformation Induced by Ground Loss

According to the derivation by Jin et al. [20], the ground vertical deformation induced by a spherical cavity in the elastic half-space can be written as:

$$u_z = \frac{V_0}{4\beta} \left(\frac{z-h}{R_1^3} + \frac{2z}{R_2^3} - \frac{(3-4\nu)(z+h)}{R_2^3} - \frac{6z(z+h)^2}{R_2^5} \right) \quad (4)$$

where V_0 denotes the volume loss induced by the spherical cavity, z denotes the point coordinate in the z -axis (vertical direction), h denotes the distance between the ground surface ($z = 0$) to the sphere center, ν denotes the Poisson's ratio $R_1 = \sqrt{r^2 + (z-h)^2}$ and $R_2 = \sqrt{r^2 + (z+h)^2}$, where r denotes the radial distance from any point to Z -axis in the half-space. Equation (4) was presented based on the virtual image technique and the harmonic function defined by Kassir and Sih [21], and more details about it can be found in [20].

For general subway tunnels, their slopes are usually required to be gentle enough to meet train operation. Thus, the shield buried depth can be simplified as a fixed value within a finite driving length. Figure 7 shows the simplified ground loss distribution along the shield tunneling axis. As drawn in Figure 7, by integrating the Green functions of

Equation (4) along the tunnel length from $-\infty$ to $-S$, the ground deformation induced by ground loss can be written as:

$$u_z^V = \int_{-\infty}^{-S} V(x, z) f_z(x, y - \xi, z) d\xi \tag{5}$$

where u_z^V denotes the vertical ground displacement, S denotes the shield length, $V(x, z)$ denotes the area of ground loss in a tunnel section, and f_z denotes the Green functions determined by Equation (4).

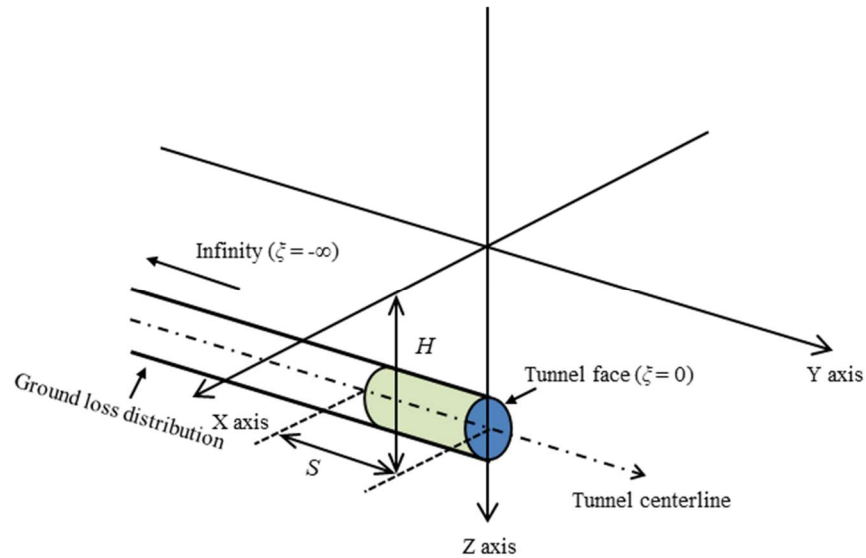


Figure 7. Ground loss distribution along the shield tunneling axis.

As described in Equation (5), the $V(x, z)$, i.e., the ground loss distribution in a tunnel section, is of great importance for final vertical ground displacement. Extensive data prove that the distribution of ground losses within the tunnel cross section is nonuniform. A widely used distribution proposed by Loganathan and Poulos [9] is suggested for calculation, which can be expressed as:

$$V(x, z) = V_l \exp\left(-\frac{1.38x^2}{(H + R)^2} - \frac{0.69z^2}{H^2}\right) \tag{6}$$

where V_l is the volume loss, H is the shield buried depth, and R is the shield buried radius. The statistical results of V_l based on local empirically derived data can provide a good reference for Equation (5), for example, the database in Figure 4 for water-rich soft strata.

Finally, the vertical deformation induced by ground loss is obtained by introducing Equation (6) into Equation (5):

$$u_z^V = \frac{V(x, z)}{4\pi} \left\{ \frac{(H-z)(R_1-y')}{r_1^2 R_1'} - \frac{2z(z+H)^2 [y'(3R_2^2 - y'^2) - 2R_2^3]}{r_2^4 R_2'^3} + \frac{[(3-4\nu)(z+H) + 2H](R_2 - y') - 2(R_2 - y')(z+H)}{r_2^2 R_2'} \right\} \tag{7}$$

where $R_1' = \sqrt{x^2 + y'^2 + (z - H)^2}$, $R_2' = \sqrt{x^2 + y'^2 + (z + H)^2}$, $r_1 = \sqrt{x^2 + (z - H)^2}$, $r_2 = \sqrt{x^2 + (z + H)^2}$, and $y' = y + S$.

4.3. Deformation Induced by Shield Working Loads

The well-known Mindlin’s solution [22], i.e., the solution for the concentrated load-induced displacement in a semi-infinite solid, is used for predicting the deformation caused by shield working loads. An integral method based on Mindlin’s solutions was used to calculate the deformation response of the EPB shield working loads, including the support pressure, shield shell friction, and cutter head rotation.

In general, the support pressure applied by the EPB shield should be as close to the in situ earth and water pressure to reduce deformations. However, it is worth noting that the applied support pressure is not equal to the sum of earth and water pressure in most circumstances. This pressure gap between them can be viewed as an evenly distributed load on the tunnel face. By double integrating along the Green function generated from Mindlin’s solution for the support face under the polar coordinate system, the ground vertical deformation induced by the pressure gap Δp can be written as:

$$u_z^p = \int_0^R \int_0^{2\pi} \Delta p \zeta(x - \rho \cos \theta, y, z - \rho \sin \theta) d\theta d\rho \tag{8}$$

where Δp denotes the pressure gap between the support pressure and in-situ earth and water pressure, u_z^p denotes the ground vertical deformation induced by Δp , ζ denotes the Green function generated from Mindlin’s solution for the horizontal force, θ denotes the angular coordinate, and ρ denotes the radial coordinate.

When calculating the ground deformation induced by shield shell friction, the friction is assumed to be an evenly distributed load along the shield shell. Coulomb law of friction, which is by far the most popular friction model, is suggested for calculating the shield shell friction. Similar to the deformation induced by Δp , the shell friction-induced vertical deformation can be obtained by integrating along the Green function over the shield shell area:

$$u_z^f = \int_0^S \int_0^{2\pi} f \zeta(x - R \cos \theta, y - \xi, z - R \sin \theta) d\theta d\xi \tag{9}$$

where f denotes the shield shell friction and can be expressed as $f = \mu F_n$, in which μ is the friction coefficient, and F_n denotes the normal stress between shield shell and soil. A summary of the friction coefficient μ can be obtained from [23] for both clayey and sandy soils.

According to the cutter head torque collected from the data acquisition system, the load stress acting on the tunnel face can be derived as:

$$q = \frac{3T}{2\pi R^3} \tag{10}$$

where q denotes the load stress acting on the tunnel face, and T denotes the cutter head torque. Then the displacement induced by cutter head rotation can be written as:

$$u_z^q = \int_0^R \int_0^{2\pi} q \rho \sin \theta \zeta(x - \rho \cos \theta, y, z - \rho \sin \theta) + q \rho \cos \theta \zeta(x - \rho \cos \theta, y, z - \rho \sin \theta) d\theta d\rho \tag{11}$$

where ζ denotes the Green function generated from Mindlin’s solution of the vertical force.

Finally, by superimposing all of the preceding components, the short-term ground deformation during shield driving can be obtained:

$$U_z = u_z^V + u_z^p + u_z^f + u_z^q \tag{12}$$

5. Case Study in Changzhou

5.1. Description of the Tunnel Project

Figure 8 shows a case history in Changzhou where the new twin shield-driven tunnels were excavated. The construction project links South Street Station and Cultural Palace

Station. Figure 8a shows a plan view of the studied section. Two EPB shield machines with a diameter of 6.34 m were employed for construction from South Street Station to Cultural Palace Station. The total length of the tunnel is 656.2 m, and the right tunnel was first constructed. A geological profile is presented in Figure 8b, revealing that the tunnels are mostly located in clay sublayer ($\textcircled{6}_3$) with a buried depth ranging from 17.7 to 28.2 m.

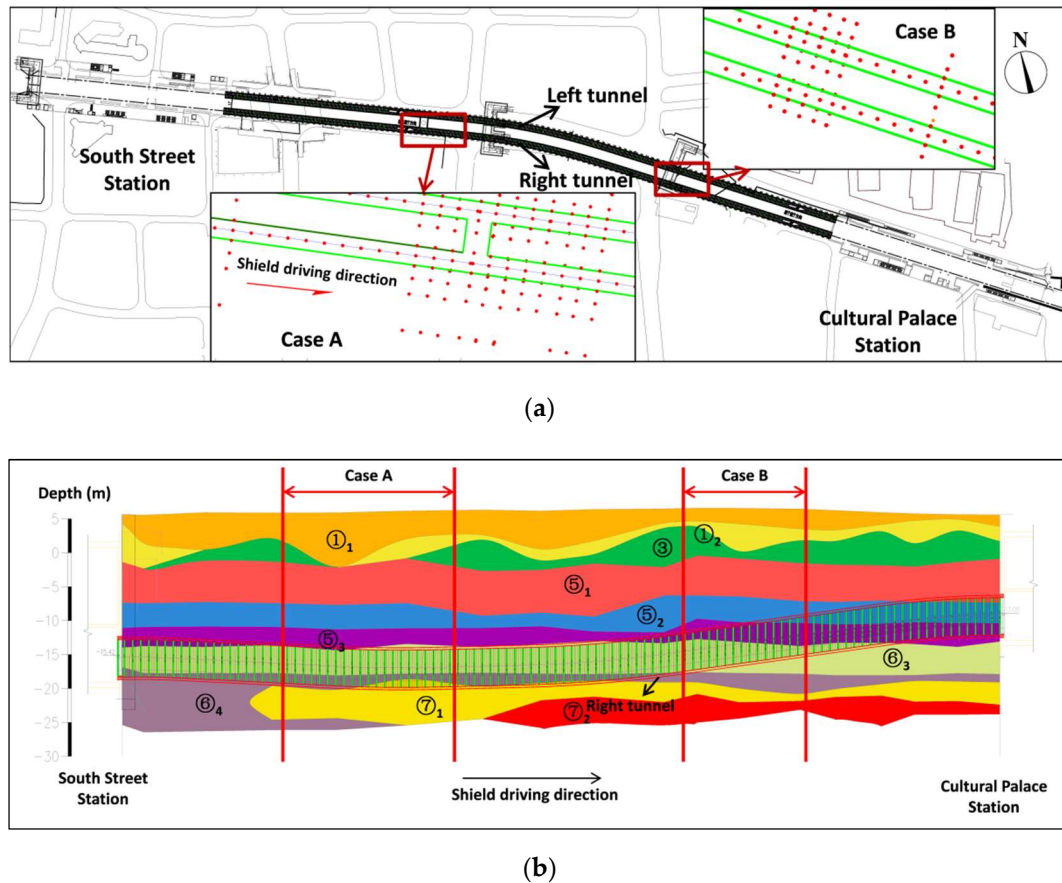


Figure 8. Shield tunnel between South Street station and Cultural Palace station. (a) plan view, (b) longitudinal tunnel sectional view.

After the right shield machine was launched from the South Street Station, the ground surface deformations were regularly monitored. Two representative monitoring cases, namely case A and case B, were selected to validate the proposed prediction method on the short-term ground deformation. As shown in Figure 8a, case A was approximately 150–200 rings distance from the South Street Station, where a total of 11 sections were set in this area, and the distance between every two sections was 6.0 m. Case B was approximately 210–350 rings distance from the South Street Station, with a total of seven sections set in this area. A total of seven monitoring points, i.e., SD1–SD7 from left to right, were arranged in each section at different distances (8 m, 3 m, 0 m, 3 m, 7 m, 12 m, and 24 m) from the tunnel centerline.

5.2. Prediction of the Ground Surface Deformations

Table 1 shows the input parameters for displacement calculation of case A. Actual geometric sizes in case A were considered for H , R , and S . The volume loss V_l was calculated and estimated based on the monitoring data of Ring 150. The E and ν were collected from $\textcircled{6}_3$ clay sublayer in the geological exploration report. The cutter head torque T was collected from the data acquisition system equipped on the shield machine, and Δp and f were the estimation results according to the thrust force of the shield. On the basis of the

parameters in Table 1, the ground deformations calculated from the proposed prediction method were obtained.

Table 1. Input parameters for displacement calculation.

<i>H</i> (m)	<i>R</i> (m)	<i>V_I</i> (%)	<i>S</i> (m)	<i>v</i>	<i>E</i> (MPa)	Δp (kPa)	<i>f</i> (kPa)	<i>T</i> (kN·m)
22	3.17	0.88	9	0.35	11	40	40	2570

Figures 9–12 present the calculated components of short-term ground deformations induced by shield driving, respectively, in which the Z-axis is taken as the vertical direction, Y-axis is taken as the shield driving direction, $Y = 0$ is where the tunnel face is located, and the X-axis is taken as the horizontal direction. As shown in Figure 9, the maximum surface settlement induced by the ground loss is 5.9 mm, and the settlement basin is mainly located in the region of $-20 \leq X \leq 20$ and $Y \leq -9$, that is, behind the shield tail. As shown in Figures 10 and 11, the vertical displacements caused by the support pressure and the shell friction are similar in shape. A spatial protrusion in the range of $0 \leq Y \leq 20$ and a settlement basin in the range of $-20 \leq Y \leq 0$ are both observed. The maximum displacements caused by the shell friction and support pressure are 2.7 mm and 0.06 mm, respectively, which indicates that the shell friction *f* has a greater effect on the short-term ground deformations. As shown in Figure 12, the contribution of the cutter head rotation to the surface displacement is extremely small, with a maximum displacement of 0.002 mm, which is almost negligible.

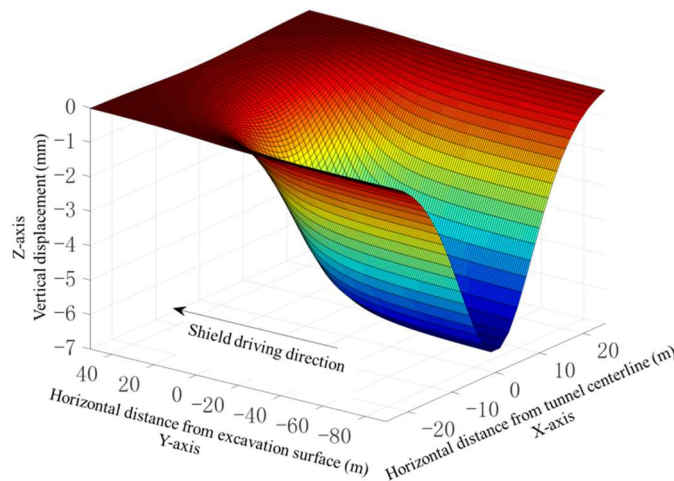


Figure 9. Ground movements induced by ground loss.

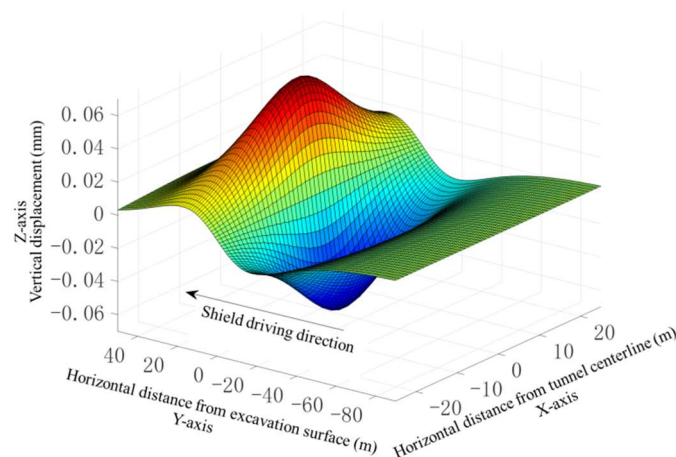


Figure 10. Ground movements induced by support pressure.

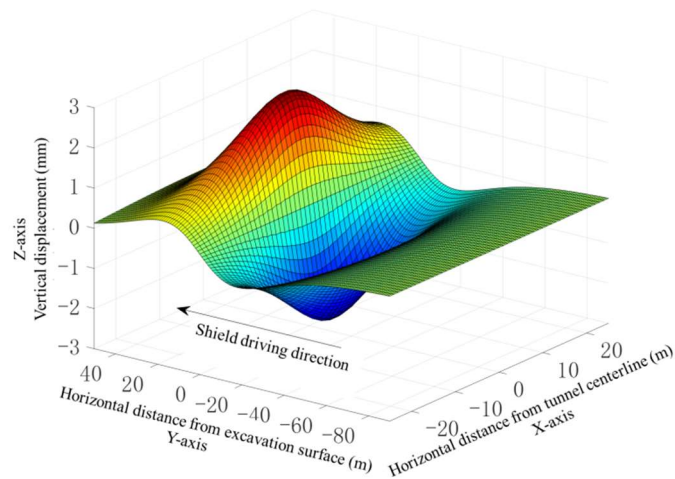


Figure 11. Ground movements induced by shield shell friction.

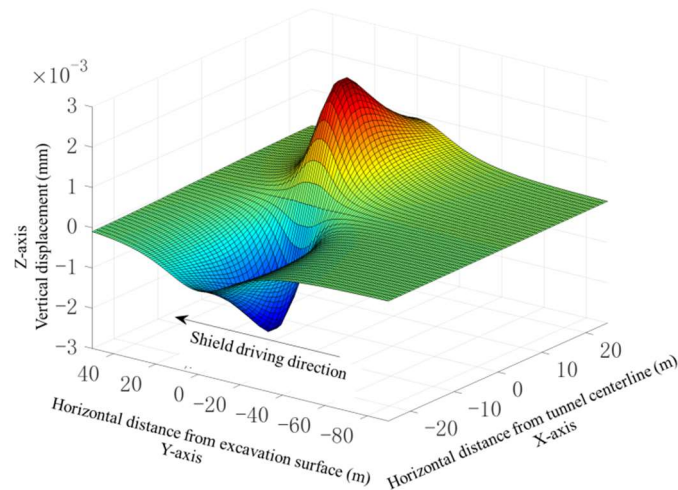


Figure 12. Ground movements induced by cutter head rotation.

5.3. Comparison between Predicted and Monitored Results

By superimposing all the displacement components in Figures 9–12, the total ground surface deformation profile of case A can be obtained. Then the predicted total deformation was tested against the field monitored results, and the comparison results are shown in Figure 13. In general, the comparison between them shows a good agreement. As presented in Figure 13, the ground surface first rises ahead of the shield machine and then collapses behind it. A maximum positive displacement of about 2 mm is observed in the range of $0 < Y < 40$, and a maximum negative displacement of about 6 mm is observed in the range of $-40 < Y < 0$. As shown in Figure 14, three columns of monitoring points, i.e., the SD3, SD4, and SD5 in Figure 13b, are selected for the comparison of longitudinal settlement in case A, of which the SD3 monitoring point is located directly above the tunnel centerline. It can be seen that in the range of the $-20 < Y < 40$, the prediction results show a great agreement with the monitoring results. However, in the range of $-100 < Y < -20$, the predicted value is lower than the monitored value. This can be attributed to the consolidation and settlement of the water-rich soft strata in the Changzhou area. After the soil layer is disturbed by shield tunneling, the excess pore water pressure gradually dissipates, resulting in long-term settlement. The empirical method proposed in Section 3 can be used to predict this long-term settlement.

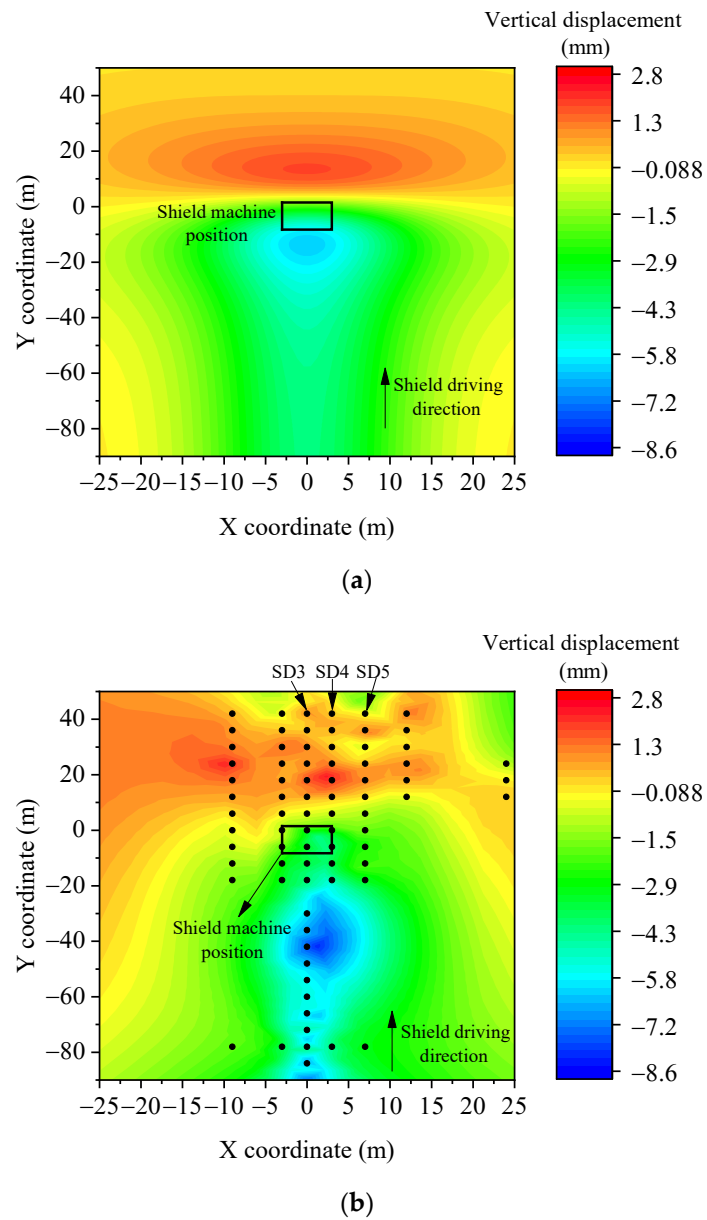


Figure 13. Comparison of predicted and monitored ground surface displacement in case A. (a) predicted displacement; (b) monitored displacement.

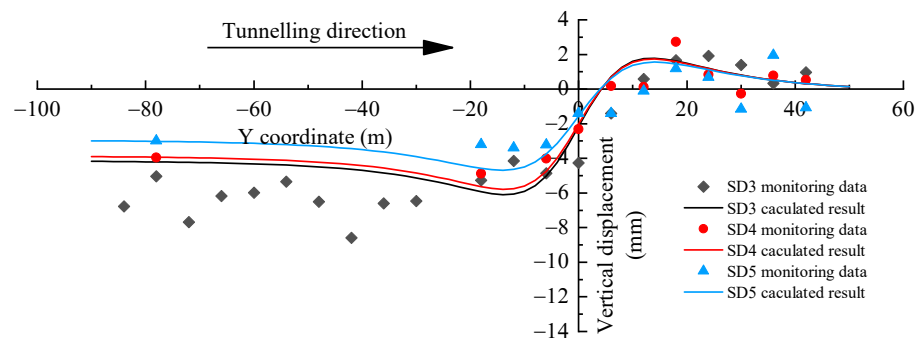


Figure 14. Comparison of predicted and measured longitudinal ground displacement in case A.

The comparison of predicted and monitored ground surface displacement in case B was obtained using the same superposition method as in case A, as shown in Figure 15. It can be seen that the comparison results show a good agreement. The ground surface first presents an uplift ahead of the shield machine and then subsides behind it. Positive displacement was observed within the region of $-10 < x < 10$ and $0 < y < 10$, whereas negative displacement was observed within the region of $-20 < x < 20$ and $y < 0$. Figure 16 shows the comparison results of longitudinal ground displacement in case B. A substantial displacement change was observed within the region of $-10 < y < 10$. Compared with Figure 15, Figure 16 shows a sharper deformation shift and a larger maximum settlement, which can be attributed to the shallower burial depth of Case B. This indicated that the influence of shield working loads on the surface deformation is more obvious when buried to a shallow depth.

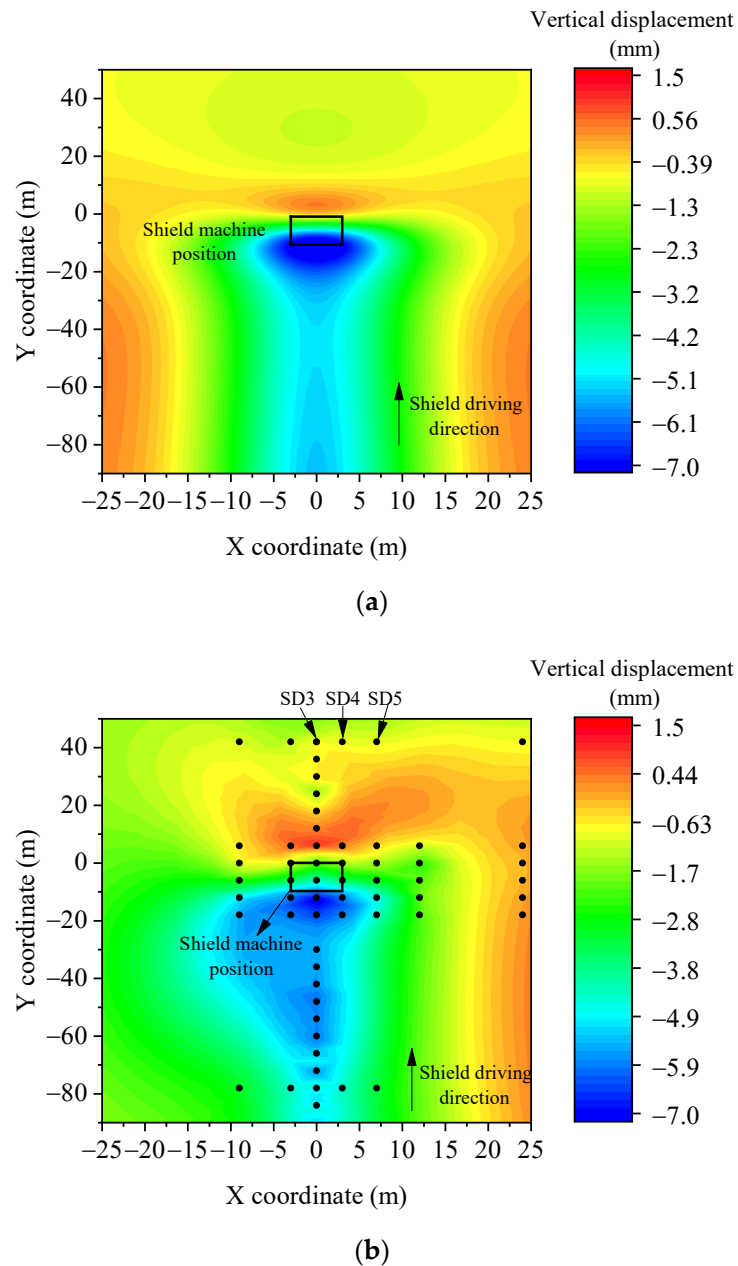


Figure 15. Comparison of predicted and monitored ground surface displacement in case B. (a) predicted displacement; (b) monitored displacement.

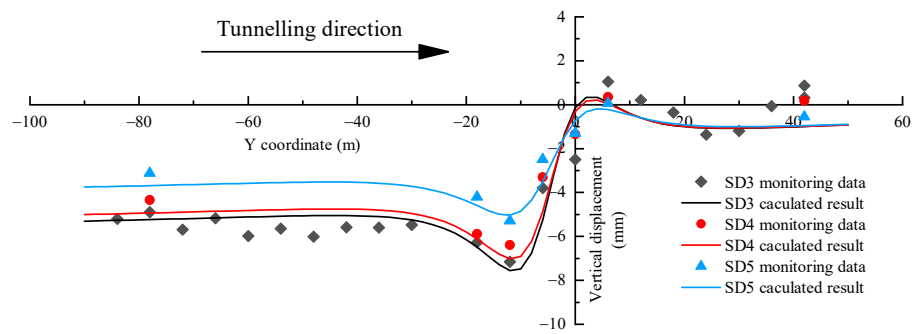


Figure 16. Comparison of predicted and measured longitudinal ground displacement in case B.

6. Discussion

This paper developed a method for estimating long-term and short-term ground deformation induced by shield driving. The long-term settlement can be calculated by using the classic Gaussian-type displacement profile. The fundamental issue with its application lies in the representational value of the prediction parameters (i.e., volume loss and trough width parameter). At the same time, the highly empirical nature of the parameters, as well as the context of the local geotechnical conditions, should also be taken into account. The variability of these prediction parameters cannot be ignored and should be carefully considered when selecting reasonable values. In this study, detailed statistics results about the prediction parameters, based on experiences obtained from Changzhou, are given, and they can provide rational guidance in predicting the long-term settlement in similar water-rich soft strata. In addition, an analytical method for predicting short-term ground deformation induced by shield driving is also presented in this paper. The prediction of short-term deformation is of great importance for the cases where differential settlements need to be considered, such as when assessing the safety of ground buildings closely spaced.

The use of empirical and analytical methods is sufficient to estimate the ground settlements in most cases of EPB shield tunnels. Compared to establishing a complicated numerical model, calibrating the existing model based on local empirical data from real-scale projects is more reasonable and acceptable.

7. Limitations and Future Works

However, it should be emphasized that the recommendations in this paper are only applicable to similar geological conditions and the cases using the EPB shield tunneling technology. The following concerns and prospective study topics will be examined in the future:

Compilation of a wider database of case studies in similar geological conditions—the database in Figures 4 and 5 is only a fraction of the experience with tunnel construction of Changzhou Metro Lines No.1 and No.2. The authors intend to expand this database as new case studies become available;

Subsurface ground movements—because the analysis conducted in this paper was based solely on data from ground surface settlements, analyzing subsurface ground movements is a suitable next step in the future. This might provide a better understanding of the variations in the ground loss that occurs when deformations travel from the tunnel to the surface. On that basis, more precise advice on the tunneling impact on subsurface infrastructure could be offered.

8. Conclusions

This study established an empirical and analytical method for predicting the long-term and short-term ground deformation induced by shield driving. The proposed method is

compared with the field measurements gathered at a tunnel project in Changzhou. The following conclusions are drawn:

- (a) Based on the statistical results of the water-rich soft soil in Changzhou, the ground loss V_l is located in the 0.1–0.75% range, and the trough width parameter K is in the 0.3–0.7 range;
- (b) The proposed analytical model considering both the ground loss and shield working loads shows a great agreement with the monitoring results within the range of the 40 m ahead of, to 20 m behind, the excavation face;
- (c) The ground loss and shell friction play an important role in the short-term ground deformations, and the effect of the cutter head torque is not worth paying attention to and can even be ignored. The effect of the support pressure is also not obvious, but it lies in a good control strategy for it;
- (d) The proposed method in this paper provided a satisfactory estimate of the long-term and short-term ground movement. A wider database is suggested to be expanded as new case studies become available.

Author Contributions: Y.Y. and X.L., conceptualization, methodology, project administration, and writing original draft; D.J., X.J. and H.L., data collection, plotting curves, analysis, and review. All authors have read and agreed to the published version of the manuscript.

Funding: The support from the Fundamental Research Funds for the Central Universities (No. 2021YJS129) is acknowledged.

Institutional Review Board Statement: Not applicable.

Informed Consent Statement: Not applicable.

Data Availability Statement: The data used to support the findings of this study are available from the corresponding author upon request.

Acknowledgments: The support from the Fundamental Research Funds for the Central Universities (No. 2021YJS129) is acknowledged.

Conflicts of Interest: The authors declare no conflict of interest.

References

1. Li, X.; Yang, Y.; Li, X.; Liu, H. Criteria for Cutting Head Clogging Occurrence during Slurry Shield Tunneling. *Appl. Sci.* **2022**, *12*, 1001. [[CrossRef](#)]
2. Yang, Y.; Li, X.; Li, X. Shear strength and compression coefficient for conditioned sand subjected to earth chamber stress levels. *Adv. Mater. Sci. Eng.* **2018**, *2018*, 1–11. [[CrossRef](#)]
3. Yang, Y.; Li, X.-G.; Su, W.-L. Experimental Investigation on Rheological Behaviors of Bentonite-and CMC-Conditioned Sands. *KSCE J. Civ. Eng.* **2020**, *24*, 1914–1923. [[CrossRef](#)]
4. Jin, D.; Yuan, D.; Li, X.; Zheng, H. Analysis of the settlement of an existing tunnel induced by shield tunneling underneath. *Tunn. Undergr. Space Technol.* **2018**, *81*, 209–220. [[CrossRef](#)]
5. Peck, R.B. Deep excavations and tunnelling in soft ground, Proceedings of 7th International Conference on Soil Mechanics and Foundation Engineering State of the Art Report. *Proc. 7th ICSMFE* **1969**, *1969*, 225–290.
6. Bloodworth, A.G. *Three-Dimensional Analysis of Tunnelling Effects on Structures to Develop Design Methods*; University of Oxford: Oxford, UK, 2002.
7. Avgerinos, V.; Potts, D.M.; Standing, J.R.; Wan, M. Predicting tunnelling-induced ground movements and interpreting field measurements using numerical analysis: Crossrail case study at Hyde Park. *Géotechnique* **2018**, *68*, 31–49. [[CrossRef](#)]
8. Mair, R.J.; Taylor, R.N.; Bracegirdle, A. Subsurface settlement profiles above tunnels in clays. *Geotechnique* **1993**, *43*, 315–320. [[CrossRef](#)]
9. Loganathan, N.; Poulos, H.G. Analytical prediction for tunneling-induced ground movements in clays. *J. Geotech. Geoenvironmental Eng.* **1998**, *124*, 846–856. [[CrossRef](#)]
10. Chapman, D.N.; Ahn, S.K.; Hunt, D.V. Investigating ground movements caused by the construction of multiple tunnels in soft ground using laboratory model tests. *Can. Geotech. J.* **2007**, *44*, 631–643. [[CrossRef](#)]
11. Moussaei, N.; Khosravi, M.H.; Hossaini, M.F. Physical modeling of tunnel induced displacement in sandy grounds. *Tunn. Undergr. Space Technol.* **2019**, *90*, 19–27. [[CrossRef](#)]
12. Do, N.A.; Dias, D.; Oreste, P.; Djeran-Maigre, I. Three-dimensional numerical simulation of a mechanized twin tunnels in soft ground. *Tunn. Undergr. Space Technol.* **2014**, *42*, 40–51. [[CrossRef](#)]

13. Fu, J.; Yang, J.; Klapperich, H.; Wang, S. Analytical prediction of ground movements due to a nonuniform deforming tunnel. *Int. J. Geomech.* **2016**, *16*, 04015089. [[CrossRef](#)]
14. Hasanipanah, M.; Noorian-Bidgoli, M.; Jahed Armaghani, D.; Khamesi, H. Feasibility of PSO-ANN model for predicting surface settlement caused by tunneling. *Eng. Comput.* **2016**, *32*, 705–715. [[CrossRef](#)]
15. Ministry of Water Resources of the People's Republic of China (MWRC). *Specification of Soil Test (SL237–1999)*; China Water Power Press: Beijing, China, 1999. (In Chinese)
16. BSI British Standards. *Methods of Test for Soils for Civil Engineering Purposes (BS 1377)*; British Standards Institution: Milton Keynes, UK, 1990.
17. O'Reilly, M.P.; New, B.M. Settlements above tunnels in the United Kingdom—their magnitude and prediction. In Proceedings of the 3rd International Symposium; Jones, M.J., Ed.; IMM: London, UK, 1982; pp. 173–181.
18. McCabe, B.; Orr, T.; Reilly, C.; Curran, B. Settlement trough parameters for tunnels in Irish glacial tills. *Tunn. Undergr. Space Technol.* **2012**, *27*, 1–12. [[CrossRef](#)]
19. Leca, E.; New, B. Settlements induced by tunneling in soft ground. *Tunn. Undergr. Space Technol.* **2007**, *22*, 119–149.
20. Jin, D.; Shen, X.; Yuan, D. Theoretical analysis of three-dimensional ground displacements induced by shield tunneling. *Appl. Math. Model.* **2020**, *79*, 85–105.
21. Kassir, M.K.; Sih, G.C. *Mechanics of Fracture 2: Three-Dimensional Crack Problems: A New Selection of Crack Solutions in Three-Dimensional Elasticity*; Noordhoff International Publishing: Leyden, The Netherlands, 1975.
22. Mindlin, R.D. Force at a Point in the Interior of a Semi-Infinite Solid. *Physics* **1936**, *7*, 195–202. [[CrossRef](#)]
23. Yang, Y.; Li, X.; Jin, D.; Su, W.; Mao, J. Transient temperature field model for a cutterhead during slurry shield tunneling. *Tunn. Undergr. Space Technol.* **2021**, *117*, 104128. [[CrossRef](#)]